Bull. Chem. Soc. Ethiop. **2027**, 41(1), 219-238.
DOI: https://dx.doi.org/10.4314/bcse.v41i1.15

ISSN 1011-3924
Printed in Ethiopia
Online ISSN 1726-801X
© 2027 Chemical Society of Ethiopia and The Authors

COMPUTATIONAL INVESTIGATION ON THE MOLECULAR AND ELECTRONIC STRUCTURE OF THE INTERACTION OF THIOPHENE WITH VARIOUS TOXIC GASES

Haripriya P.[1], Amrutha R.[2]*, Chandran P.[3]

[1]Research Scholar, Bharathiar University, Coimbatore, PIN-641046, Tamil Nadu, India
[2]Department of Physics, KCG College of Technology, Rajiv Gandhi Salai, Karapakkam, Chennai, PIN-600097, Tamil Nadu, India
[3]Madras Christian College, Tambaram East, Tambaram, Chennai, PIN-600059, Tamil Nadu, India

(Received October 15, 2024; Revised September 2, 2026; Accepted November 3,2026)

ABSTRACT. Density functional theory calculations were used to examine adsorption of carbonyl fluoride (COF_2), cyanogen chloride (CNCl), and boron trifluoride (BF_3) on thiophene using B3LYP/6-31+G(d) and ωB97XD/6-31+G(d). All complexes exhibit weak exothermic adsorption consistent with physisorption. Counterpoise-corrected interaction energies at B3LYP are −2.259, −3.389, and −4.730 kJ/mol for COF_2, CNCl, and BF_3, respectively; corresponding ωB97XD values are −11.970, −10.042, and −16.736 kJ/mol. Adsorption changes the dipole moment of thiophene from 0.5469 D to 1.2527, 3.4267, and 0.6534 D, respectively. COF_2 reduces the calculated HOMO–LUMO gap from 5.97 to 5.131 eV, whereas CNCl and BF_3 yield gaps of 5.972 and 6.00 eV. Mulliken and natural bond orbital analyses indicate small intermolecular charge transfers, and the calculated desorption times are short under the assumed conditions. BF_3 has the strongest calculated binding, while COF_2 produces the largest orbital-gap response. These molecular-level predictions support further investigation of thiophene-based materials for toxic-gas sensing, although device performance requires experimental validation.

KEY WORDS: Thiophene, Toxic gases, Density functional theory, Interaction energy, Charge transfer, Molecular orbitals

INTRODUCTION

The release of toxic gases into the environment through industrial processes, accidental leakage, or the handling of chemical-warfare agents poses a serious threat to human health and environmental safety, and the rapid and accurate detection of such hazardous species at low concentrations has become an indispensable requirement [1]. Because several of these substances can cause severe, sometimes fatal, health effects even at low exposure levels [2], reliable gas monitoring is essential not only for occupational safety and public-health protection but also for preventing the chronic effects of low-level exposure that may otherwise go unnoticed. Ideal gas sensors must therefore combine high sensitivity and selectivity with fast response and recovery, low power consumption, and chemical stability, ideally at room temperature.

A wide range of sensing technologies has been developed to meet this need, with semiconductor-based materials the most extensively studied. Metal oxides are frequently the materials of first choice because of their ease of fabrication, low cost, high sensitivity, and stability, but they suffer from low selectivity and a requirement for high operating temperatures [3]. Carbon nanotubes are chemically and mechanically stable and respond sensitively to NO and NH_3, yet they generally need dopants or functionalization to sense other gases, while emerging two-dimensional materials are still being developed for practical devices [3]. Conducting polymers offer a complementary set of advantages: they operate at or near ambient temperature,

*Corresponding author. E-mail: amrutha@kcgcollege.com
This work is licensed under the Creative Commons Attribution 4.0 International License

are flexible and easy to process, and respond to a wide range of toxic gases and organic vapors, although their response can be affected by humidity [3, 4]. Indeed, organic-semiconductor sensors based on conducting polymers were recognized early on for their sensitivity to toxic gases and their ability to operate close to room temperature, in contrast to metal-oxide devices [4].

In their chemiresistive form, conducting polymers operate on the principle of a change in the electrical resistance of the sensing layer upon exposure to an analyte [5]. Thiophene-based conducting polymers are particularly promising in this regard. Printable polythiophene sensor arrays have been shown to respond to volatile organic compounds down to concentrations of 10 ppm [6], regioregular polythiophene copolymers give fast and fully reversible room-temperature responses to organic vapors [7], and a thiophene polymer bearing oligoethylene glycol side chains has demonstrated ultrahigh sensitivity toward NO_2, with a response of $3.58 \pm 2.38 \times 100\%$ at the 20 ppb level [5]. These experimental demonstrations establish thiophene-based materials as realistic sensing platforms and motivate a molecular-level understanding of how small gaseous analytes perturb the electronic structure of the thiophene unit.

Density functional theory is now a well-established, cost-effective tool for screening candidate sensing materials and for rationalizing adsorption mechanisms before device fabrication. For conjugated polymers, the sensing behavior toward a given analyte can be modeled reasonably using the monomer unit alone, which reduces computational cost while still reproducing the essential physics of the interaction [8, 9]. DFT studies of polypyrrole in its neutral and doped forms have shown it to be more sensitive to NH_3 than to CO_2 or CO on the basis of interaction energies, charge transfer, and frontier-orbital analysis [8]. Likewise, emeraldine-salt polyaniline showed a greater response selectivity toward NH_3 than toward CO_2 and CO [10], and a dianiline model of polyaniline was found to physisorb SO_2 and SO_3 with BSSE-corrected adsorption energies of −18.2 and −62.9 kJ/mol, respectively [11]. As the smallest model of polythiophene, terthiophene has been investigated against atmospheric gases including CO, CO_2, SO_2, and CH_3OH, with interaction energies between −5.3 and −16.7 kJ/mol characteristic of physisorption [9], while comprehensive surveys of polypyrrole across more than a dozen analytes identified SO_2 and SO_3 as the most responsive species [12]. Studies of related thiophene systems have reached similar conclusions: PEDOT physisorbs SO_3, NH_3, NO_2, and H_2S with adsorption energies of −6.02 to −13.32 kcal/mol [13], and a diamine-functionalized terthiophene exhibits particular selectivity toward SO_2 among SO_3, SO_2, HCN, and CO_2 [14]. Most relevant to the present work, a DFT study of polypyrrole interacting with toxic heterocarbonyl gases including carbonyl fluoride showed that these analytes modify the structural and optoelectronic properties of the polymer, with reductions in the energy gap signaling high sensitivity [15]. Collectively, these studies demonstrate that conducting-polymer sensors merit systematic computational investigation against industrial toxic gases, and that thiophene in particular has not yet been examined for several highly hazardous species.

The three analytes considered in this study are all substances of serious occupational and public-health concern. Carbonyl fluoride (COF_2), a toxic heterocarbonyl gas closely related to phosgene, can cause severe skin and eye irritation and burns, irritation of the nose and throat, and injury to the liver and kidneys; the NIOSH recommended exposure limit is 2 ppm as an 8-hour time-weighted average and 5 ppm as a 15-minute short-term limit [16], and health-based exposure recommendations have been derived from its toxicological similarity to hydrogen fluoride [17]. Cyanogen chloride, one of the agents historically stockpiled as a military choking gas [2], is a highly toxic blood agent: it is converted in the body to hydrogen cyanide, which blocks cellular energy metabolism and leads to respiratory failure [2]. It combines with trivalent iron in cells, impairing normal respiration and causing asphyxia, and can produce dizziness, nausea, and vomiting, with paralysis and death within minutes in severe cases [1]. Because it is classified alongside hydrogen cyanide among the principal blood agents [18], rapid and real-time detection of CNCl is a documented priority [1]. Boron trifluoride (BF_3) is a pungent, corrosive gas that irritates the eyes, skin, and respiratory tract and can produce burns, dyspnea, and pulmonary

edema, with an OSHA and NIOSH ceiling limit of 1 ppm [16]; four-hour inhalation studies in rodents established respiratory irritation at 74.4 mg/m³ with a no-observed-adverse-effects level of 24.6 mg/m³ [19], and chronic exposure can cause nosebleeds, osteosclerosis, anemia, and weight loss. Given that all three gases can cause severe, sometimes fatal, effects at low concentrations, the development of inexpensive, reusable sensing materials for their detection carries substantial public-health significance.

Although thiophene-based systems have been modeled against a range of common gases, their interaction with the highly toxic species COF_2, CNCl, and BF_3 has not been systematically explored, and the effect of these analytes on the frontier-orbital gap of thiophene a key transduction parameter for chemiresistive sensing [5] remains largely unknown. A central objective of this work is the hitherto unexplored determination of the decrease in the energy gap of thiophene upon interaction with COF_2, which increases the electrical conductivity of the monomer and makes it suitable for use in organic cells and organic light-emitting diodes; the perturbation of the HOMO and LUMO energies produces a significant change in the energy gap, indicating that thiophene becomes less chemically stable and more reactive after COF_2 adsorption. In contrast, complexation with CNCl and BF_3 slightly increases the energy gap, rendering thiophene more chemically stable and less reactive. Since the resulting change in conductivity is one of the most direct observable signatures of gas sensing, the specific objectives of this study are: (i) to establish, from counterpoise-corrected interaction energies, that all three analytes are physisorbed on thiophene through van der Waals interactions; (ii) to quantify the charge transfer and dipole-moment changes accompanying adsorption; (iii) to evaluate the sensing ability of thiophene from interaction-energy, energy-gap, and recovery-time analyses; and (iv) to identify which of the three analytes thiophene detects with the highest sensitivity.

COMPUTATIONAL METHODS

Computational details

All calculations were performed in the gas phase using the Gaussian 09 quantum chemistry package [20], and molecular structures were built and inspected with GaussView 5.0 [21], with molecular orbital and electrostatic-potential plots prepared using Gabedit 2.5.0 [22]. Natural bond orbital analysis was carried out with the NBO 3.1 module implemented in Gaussian. Geometry optimization of isolated thiophene, the three analyte molecules (COF_2, CNCl, and BF_3), and the three thiophene–analyte complexes was carried out at the density functional theory level using the B3LYP hybrid functional [23] with the 6-31+G(d) basis set, which is well established to yield reliable results for the structural and electronic parameters of conjugated organic molecules owing to its exchange–correlation treatment. To verify the adequacy of the chosen level of theory, the computed bond lengths and bond angles of thiophene were compared with available experimental values and were found to be in good agreement, substantiating the accuracy of the basis set. For comparative purposes, all structures were additionally re-optimized at the ωB97XD/6-31+G(d) level of theory [24] in combination with Grimme's D2 dispersion model [25]. From the resulting relaxed minima, structural parameters, dipole moments, interaction energies, counterpoise-corrected energies, Mulliken charge analysis, NBO analysis, frontier molecular orbitals, energy gaps, and molecular electrostatic potential surfaces were calculated for the monomer and all complexes.

Selection of the level of theory

B3LYP, formed from Becke's three-parameter exchange functional and the Lee–Yang–Parr correlation functional [23], was selected as the primary level of theory because it combines accuracy with low computational cost for electronic-structure parameters and remains the most

extensively benchmarked functional in computational studies of conducting-polymer gas sensors, including earlier DFT investigations of polypyrrole and polyaniline at the B3LYP/6-31G(d) level [8, 10]. Comparable adsorption studies adopt the same division of labor, using B3LYP for electronic parameters and reactivity descriptors while reserving a dispersion-corrected functional for adsorption energetics [26]. The 6-31+G(d) basis set was chosen because the diffuse functions provide the long-range electron density required to describe weakly bound van der Waals complexes, while the polarization functions permit deformation of the atomic orbitals during complexation.

The principal limitation of B3LYP is that it does not account for dispersion, i.e., the correlation energy arising from fluctuations in the charge distribution of a molecular system, which are precisely the forces that dominate weak physisorption. The ωB97XD functional [24] a range-separated version of Becke's 97 functional comprising 22% Hartree–Fock exchange at short range and 100% at long range, augmented with Grimme's empirical D2 dispersion correction [25] was therefore used for comparative re-optimization and for computing the interaction energies. This choice is supported by benchmark studies in which ωB97-based functionals with dispersion corrections reproduce CCSD(T) reference curves most accurately for the physisorption of small molecules (N_2, CO_2) on aromatic surfaces [27]; the same dispersive physics governs the adsorption of organic molecules on sp^2-carbon and heteroaromatic frameworks, where London-type forces amount to roughly 60% of the attractive interaction [28]. It should be noted that for very small systems comprising 4-8 atoms, inclusion of dispersion corrections has been reported to increase the root-mean-square interaction-energy error; consequently, the B3LYP and ωB97XD results are best interpreted jointly as bracketing the true interaction energy of each complex, and both are reported throughout.

Justification of Grimme's D2 dispersion correction

Structural screening of the complexes showed that the analytes approach thiophene at large nonbonding contact distances (2.60-4.22 Å), and the intermolecular NBO second-order stabilization energies are small (≤ ~2.1 kcal/mol), placing all three interactions firmly in the dispersion-dominated physisorption regime. Hybrid functionals without dispersion fail in exactly this regime, whereas empirical dispersion corrections restore the missing long-range correlation: dispersion-corrected B3LYP has been shown to outperform MP2 and to be in excellent agreement with the CCSD(T)/complete-basis-set limit for weakly bound aromatic dimers such as CO_2–benzene, with typical root-mean-square deviations below 3 kJ/mol [29], and B3LYP augmented with an empirical dispersion term markedly improves the theoretical characterization of physisorbed species wherever dispersion is crucial [30].

The D2 correction [25] is a pairwise, damped C_6R^{-6} term added to the DFT energy. It is empirical, adds negligible computational cost, and does not alter the electron density; importantly, because its gradient enters the optimization, it directly influences the equilibrium geometries significant here, since the dispersion interaction determines both the adsorption distances and the geometry perturbations that underlie the observed sensing response. For the present system, D2 was adopted specifically as implemented within the ωB97XD parameterization [24], ensuring a physically consistent long-range-corrected exchange–correlation description together with the dispersion treatment in a single functional.

Interaction energies, BSSE correction, and recovery time

The interaction energy between thiophene and each analyte was calculated from the relaxed minimum-energy structures as,

$$\mathbf{E}\text{int} = E\text{complex} - (E\text{monomer} + E\text{analyte})$$

where Ecomplex is the total energy of the optimized thiophene analyte complex, and Emonomer and Eanalyte are the total energies of the isolated thiophene and analyte molecule, respectively. The interaction energy was corrected for basis set superposition error using the counterpoise method,

$\mathbf{E}\text{int,CP} = \text{Eint} - \text{EBSSE}$

To estimate the reusable efficiency of the thiophene sensor, theoretical recovery times were calculated at 300 K using the transition-state expression

$\tau = \nu^{-1} \exp(|\text{Eb}| / K_B T)$

where ν is the attempt frequency, taken as 1 THz; E is the binding energy of the analyte on thiophene; and K_B is Boltzmann's constant.

Electronic property analyses

The extent of intermolecular charge transfer was quantified by Mulliken population analysis and corroborated by NBO analysis, in which the donor–acceptor interactions between occupied Lewis-type NBOs of one unit and vacant non-Lewis-type NBOs of the other were evaluated through second-order perturbation theory analysis of the Fock matrix in the NBO basis, using

$$^{E(2)} = \Delta Eij = q_i F(i,j)^2 \frac{qiF(i,j)2}{\epsilon j - \epsilon i}$$

where q_i is the donor orbital occupancy, ε_i and ε_j are the diagonal elements (orbital energies), and F(i,j) is the off-diagonal NBO Fock matrix element. Frontier molecular orbital energies and the resulting energy gaps were computed at the B3LYP/6-31+G(d) level for the monomer and all complexes, and total electron density isosurfaces were mapped with the molecular electrostatic potential.

RESULTS AND DISCUSSION

Overview of key findings

Three conclusions anchor the entire study. First, all three analytes COF_2, CNCl, and BF_3 are physisorbed on thiophene through weak van der Waals interactions, as evidenced by the small exothermic interaction energies (−3.115 to −6.051 kJ/mol at B3LYP and −11.340 to −18.098 kJ/mol at ωB97XD), the large nonbonding contact distances (2.60–4.22 Å), and the marginal perturbation of the internal bond lengths of thiophene. Second, the sensing response differs by analyte: complexation with COF_2 narrows the HOMO–LUMO gap from 5.97 eV to 5.131 eV, the only complex that becomes more conductive, whereas CNCl and BF_3 slightly widen the gap to 5.972 eV and 6.00 eV, stabilizing the monomer. Third, the computed recovery times are picosecond to sub-nanosecond at 300 K, indicating spontaneous desorption and full reusability of the sensor without any regeneration step. The relative sensing aptitude follows the interaction-energy ordering thiophene–BF_3 > thiophene–CNCl > thiophene–COF_2, with BF_3 giving both the most negative interaction energy and the longest (though still ultrafast) residence time.

Structural properties

Geometries of the isolated thiophene, the analytes (COF_2, CNCl, and BF_3), and the thiophene analyte complexes were optimized at the DFT B3LYP/6-31+G(d) level, and the results for the monomer were compared with the available experimental values to describe the correlation between the geometric structures and their properties. The results obtained from the DFT

calculations at the B3LYP/6-31+G(d) level are in good agreement with the experimental values, which substantiates the accuracy of the basis set. A previous DFT study of the structural and electronic properties of thiophene with COS found that the optimized geometrical parameters of the complex undergo changes in the bond lengths and bond angles compared with those of the monomer, thereby establishing the sensitivity and selectivity of the monomer toward the analyte. In the present study, the optimized structures of thiophene and thiophene with COF_2 are shown in Figures 1 and 2, respectively.

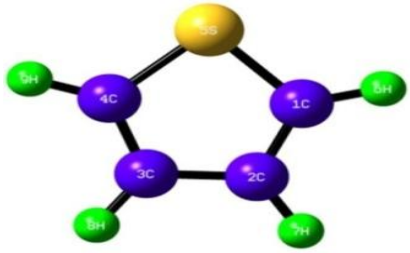


Figure 1. Optimized structure of thiophene at the density functional theory (DFT) B3LYP/6-31+G (d) level.

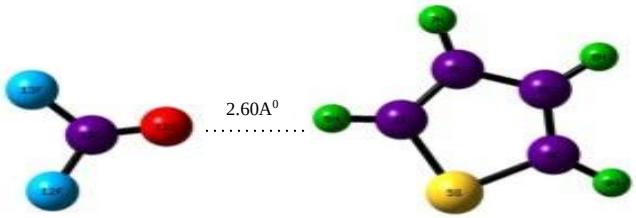


Figure 2. Optimized structure of thiophene with COF_2 at the DFT B3LYP/6-31+G (d) level. The violet, green, yellow, red, sky blue balls represent C, H, S, O, and F, respectively.

Analyzing the optimized interbond length and the various interaction bond angles of the thiophene–COF_2 complex, it is found that there is only a slight change in the bond length of thiophene after interaction with COF_2 due to van der Waals interaction between monomer and COF_2, but the bond angles vary considerably. Both the interior and exterior bond angles of COF_2 alternatively increase and decrease with respect to the monomer. The exterior bond angle ∠S5C1H6 closer to the interaction site decreases by 0.0381° whereas the other exterior bond angle ∠C2C1H6 increases by 0.1673°. According to valence shell electron pair repulsion theory, the electronegativity of both oxygen of COF_2 and sulfur of thiophene greatly affect the bond angles due to changes in the distribution of electrons after complexation. The bond angles of the complex ∠C1C2C3, ∠C3C2H7, ∠C2C3H8, ∠S5C4H9, and ∠C1S5C4 were larger than those of the monomer by 0.1089°, 0.0242°, 0.0405°, 0.1002°, and 0.092°, whereas ∠C2C1S5, ∠C1C2H7, ∠C2C3C4, ∠C4C3H8, ∠C3C4S5, and ∠C3C4H9 were smaller than those of the monomer by 0.1291°, 0.1332°, 0.0088°, 0.0318°, 0.0655°, and 0.0346°. The interaction site H6 of thiophene and O11 of COF_2 influences the geometric changes in the bond angles of the complex, and the polar nature of COF_2 arising from the electronegativity difference between oxygen and fluorine also affects the geometrical parameters largely.

For thiophene with CNCl, the intrabond lengths and bond angles calculated at the B3LYP/6-31+G(d) level correlate well with the experimental values. The optimized structure of thiophene

with CNCl is shown in Figure 3. The theoretical efforts reveal that the bond length of thiophene is fairly unaltered after adsorption with CNCl; a marginal overestimation in the C3–C4 bond length of 0.0016 Å is observed, and this particular bond length is closer to the interaction site Cl11 of CNCl. Nevertheless, the adsorption of CNCl produces significant distortion in the geometry of the bond angles of thiophene compared with COF_2. Deviations in the bond angles ∠C4C3H8, ∠C3C4H9, and ∠S5C4H9 by 0.025°, 0.054°, and 0.049° indicate that these angles are nearer to the adsorption site Cl11 of CNCl. The changes in the bond angles that involve S5 of thiophene, such as ∠C2C1S5, ∠S5C1H6, ∠C3C4S5, ∠S5C4H9, and ∠C1S5C4, produce remarkable changes of 0.0843°, 0.0043°, 0.0042°, 0.049°, and 0.1045° due to the electronegativity of sulfur during interaction with the analyte. The exterior bond angle ∠C1C2H7, far away from the interaction site, remains unchanged whereas another exterior bond angle ∠C2C1H6 closer to S5 contracts by 0.0799°. The interior bond angle ∠C1C2C3 decreases by 0.0489°, and another interior bond angle ∠C2C3C4 produces less internal strain by 0.0182°. Both exterior bond angles ∠C3C2H7 and ∠C2C3H8 are overestimated relative to the monomer by 0.0487° and 0.0398°, respectively. Studying the optimized interbond length and the various interbond angles of the thiophene–CNCl complex, the interaction distance between S5 of thiophene and Cl11 of CNCl is 4.22 Å, which supports the establishment of a van der Waals-type interaction. The interbond angles ∠C1S5Cl11 and ∠C4S5Cl11 reveal the dipole–induced dipole interaction that substantiates the nonpolar nature of thiophene and the polar nature of CNCl in the thiophene–CNCl complex.

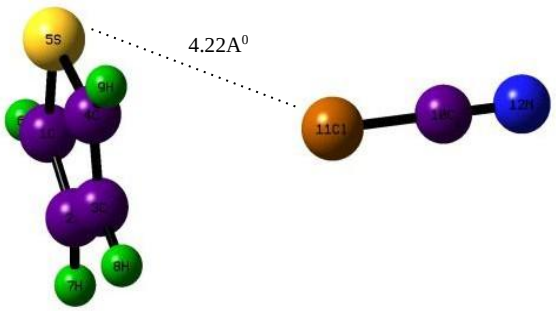


Figure 3. Optimized structure of thiophene with CNCl at the DFT B3LYP/6-31+G (d) level. The violet, green, yellow, brown, blue balls represent C, H, S, Cl, and N, respectively.

Regarding thiophene–BF_3, the optimized geometrical parameters show that the monomer bond distances alternatively increase and decrease after complexation with BF_3. The optimized structure of thiophene with BF_3 is shown in Figure 4. Geometries of the optimized complex thiophene–BF_3 reveal that the sensing response is very high and shows remarkable changes in the bond angles when compared with the other analytes. Significant variation is noticed in the C1–C2 bond length and the ∠C2C1H6 and ∠C1C2H7 exterior bond angles, and the difference in the structural parameters may be attributed to the interaction site. From the structural changes, it is clear that the interaction is a kind of van der Waals interaction. The bond angles open up for ∠S5C1H6, ∠C1C2H7, ∠C3C2H7, ∠C2C3H8, and ∠C3C4S5, and contract for ∠C2C1S5, ∠C2C1H6, ∠C1C2C3, ∠C2C3C4, ∠C4C3H8, ∠C3C4H9, ∠S5C4H9, and ∠C1S5C4. These deviations in the bond angles denote, without doubt, the sensing aptitude of thiophene toward BF_3. The three important interaction distances are between C1–B10, H6–F12, and H7–F13, having values equal to 3.36 Å, 3.14 Å, and 3.12 Å, respectively; the nonbonding interaction distance is responsible for physisorption. The various remarkable interbond angles reveal the induced dipole–induced dipole attraction, also called the London dispersion forces, that arises due to the nonpolar nature of BF_3 and the nonpolar nature of thiophene during complexation.

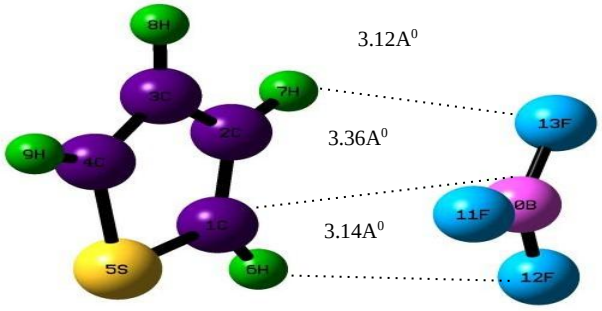


Figure 4. Optimized structure of thiophene with BF_3 at the DFT B3LYP/6-31+G (d) level. The violet, green, yellow, sky blue, and pink balls represent C, H, S, F, and B, respectively.

It is found that appreciable changes with respect to bond lengths are produced for thiophene–BF_3 complexation, whereas the changes in the bond lengths are less pronounced for the remaining thiophene–analytes (COF_2 and CNCl). The theoretical investigation of the interaction of all the analytes causes the bond angles to fluctuate to a greater extent, which results in the perturbation of the thiophene structure. The calculated results further show that the interaction does not significantly change the bond lengths of the monomer to a greater extent. This pattern — small bond-length but significant bond-angle response is the hallmark of nonbonded van der Waals contact and confirms that the geometry changes are localized at the interaction site.

Dipole moment

Adsorption increases the dipole moment of thiophene from 0.5469 D to 1.2527 D for COF_2, 3.4267 D for CNCl, and 0.6534 D for BF_3. The large increase in the CNCl complex reflects the polar nature of the C–Cl bond combined with charge transfer from thiophene to the analyte, whereas the modest change for BF_3 is consistent with dipole–induced-dipole interaction between two largely nonpolar partners. These shifts confirm that electron density is reorganized upon adsorption and provide a secondary, experimentally accessible signature of complexation.

Interaction energies and the physisorption regime

Gas adsorption is useful in determining the adsorption energy and the amount of charge transferred between the monomer and the analyte. The interaction energy between thiophene and COF_2 is exothermic and equal to −3.115 kJ/mol, clearly indicating physisorption; the minimum negative value of the interaction energy, together with the nonbonding distance of 2.60 Å between H6 of thiophene and O11 of COF_2, confirms the presence of van der Waals forces. At the ωB97XD/6-31+G(d) level, the interaction energy is −13.930 kJ/mol, somewhat higher than the B3LYP value because, for functionals describing small systems comprising 4–8 atoms, the inclusion of dispersion corrections increases the root-mean-square interaction-energy error. The counterpoise-corrected values are −2.259 kJ/mol (B3LYP) and −11.970 kJ/mol (ωB97XD), with BSSE of 0.8213 kJ/mol (0.36% of E_int) and 1.931 kJ/mol (0.16% of E_int), respectively.

For thiophene–CNCl, the interaction energy is exothermic and equal to −4.442 kJ/mol, with a nonbonding distance of 4.22 Å between S5 and Cl11; the counterpoise-corrected values are −3.389 kJ/mol (B3LYP) and −10.042 kJ/mol (ωB97XD), with BSSE of 1.089 kJ/mol (0.32% of E_int) and 1.140 kJ/mol (0.1135% of E_int). The greater interaction energy than for thiophene–COF_2 indicates a greater response of the monomer toward CNCl. For thiophene–BF_3, the interaction energy is −6.051 kJ/mol, the highest of the three, supported by the three nonbonding

distances C1–B10 = 3.36 Å, H6–F12 = 3.14 Å, and H7–F13 = 3.12 Å; counterpoise-corrected values are −4.730 kJ/mol (B3LYP) and −16.736 kJ/mol (ωB97XD), with BSSE of 1.751 kJ/mol (0.370% of E_int) and 2.257 kJ/mol (0.135% of E_int). Since ωB97XD is a range-separated version of Becke's 97 functional comprising 22% Hartree–Fock exchange at short range and 100% at long range [24], the inclusion of dispersion correction leads to chemical accuracy in the values. Three points merit emphasis: (i) the ωB97XD values are roughly 3–5 times larger in magnitude than the B3LYP values because the dispersion correction adds the long-range correlation energy that pure B3LYP omits; (ii) the ordering is consistent across both levels, giving confidence that the relative sensing aptitude (BF_3 > CNCl > COF_2) is not an artifact of a particular functional; and (iii) all interaction distances lie well beyond covalent bond lengths and are characteristic of van der Waals contact, the same physisorption behavior reported for terthiophene segments interacting with atmospheric gases [9]. Thus, with respect to interaction energy the main property governing gas-sensing behavior thiophene has the greatest response toward BF_3.

Charge analysis

The thiophene–COF_2 interaction is best explained by charge transfer, in agreement with the second-order perturbation theory analysis of the Fock matrix of thiophene with carbonyl sulfide, where the analyte was regarded as a donor NBO and thiophene as an acceptor NBO. COF_2 transfers −0.0167 e^- to thiophene by Mulliken analysis, and the same trend is observed from NBO charge transfer, with the analyte giving 0.00218 e^- to the monomer; COF_2 therefore acts as the electron donor. For thiophene–CNCl, reverse transfer of charge occurs: thiophene gives 0.0081 e^- to CNCl by Mulliken analysis, and CNCl accepts 0.00563 e^- by NBO analysis, with thiophene acting as the donor NBO and CNCl as the acceptor NBO. For thiophene–BF_3, Mulliken charge transfer of −0.0357 e^- occurs from the analyte to the monomer, whereas NBO analysis shows a reverse transfer of 0.00912 e^- from monomer to analyte with BF_3 as the donor in the Mulliken picture and the acceptor in the NBO picture. The low charge values obtained through both analyses are consistent with the low interaction energies of van der Waals type, and the charge transfer alters the electronic properties of thiophene, proving its sensing capability.

Recovery time: implications for sensor operation

The recovery time, calculated from the transition-state expression with an attempt frequency ν = 1 THz at T = 300 K, is the time required for an adsorbed molecule to desorb spontaneously and is the standard measure of sensor reusability [31, 32]. The computed values 3.47×10^{-12} to 11.31×10^{-12} s at B3LYP and 9.44×10^{-11} to 1.42×10^{-9} s at ωB97XD are remarkably short, and three implications follow.

Operational implications. Because desorption is spontaneous at room temperature, a thiophene-based device requires no thermal or light-assisted regeneration cycle between measurements. This stands in contrast to many metal-oxide and two-dimensional-material sensors, where room-temperature thermal energy is insufficient to desorb strongly bound analyte, forcing elevated-temperature operation or UV-assisted recovery at the cost of response performance [33]. Recovery times of 16 s (NO_2 on carbon nanotubes), 150 s (NH_3 on WS_2), and 240 s (NO on In_2O_3) are typical of conventional physisorption sensors [31], so the picosecond-to-nanosecond timescales obtained here imply that the thiophene sensor would support essentially continuous, real-time monitoring with effectively zero dead time.

Statistical/trade-off implications. The very short recovery time is the direct consequence of weak binding, and it deserves an honest caveat: at 300 K the equilibrium surface coverage of these analytes on thiophene will be low, and, as has been noted for other ultra-weak physisorption

systems, if the transducer relied only on mass loading such instantaneous desorption would preclude stable detection [34]. The sensing signal must therefore be read out electronically through the analyte-induced change in conductivity rather than through accumulation of adsorbed mass. This is exactly the operating principle of chemiresistive conducting-polymer sensors [4, 5], and it is why the energy-gap response discussed in Section 3.7, not the binding energy, is the decisive transduction parameter.

Functional/ordering implications. The exponential dependence of τ on the binding energy means that even small differences in E_b translate into large differences in τ: doubling the binding energy increases τ by many orders of magnitude, as observed for carbon-nanotube NO_2 sensors, where adsorption energies of −0.34 to −0.79 eV correspond to recovery times of 5 ms to 16 s, and −1.00 eV to about 12 hours [35]. Within this study, the same exponential scaling explains why the dispersion-corrected ωB97XD recovery times exceed the B3LYP values, and why BF_3, the most strongly bound analyte, shows the longest recovery time at both levels (11.31×10^{-12} s and 1.42×10^{-9} s). A longer residence time improves the probability of capturing and transducing the adsorption event, consistent with BF_3 being the easiest analyte to detect; the computed times at both levels prove the reusable efficiency of the thiophene gas sensor.

Frontier molecular orbitals and energy gap: implications for sensor design

The energies of the HOMO and LUMO and the energy gap (E_g) were calculated at the B3LYP/6-31+G(d) level; the frontier-orbital analysis is the most practically significant result of this work, because the energy gap directly controls the chemiresistive signal: electrical conductivity increases exponentially as the gap decreases ($\sigma \propto \exp(-E_g/2k_BT)$), and an increase in the gap corresponds to higher resistivity [36, 27, 38]. The relevant schematics are shown in Figures 5(a)–7(b).

COF_2: conductivity increase. COF_2 contributes to the LUMO after interaction. An increase of 0.158 eV is observed in the HOMO energy (−6.610 → −6.452 eV), and the LUMO energy decreases by 0.6813 eV (−0.6397 → −1.321 eV), narrowing the gap by 0.839 eV, from 5.97 eV to 5.131 eV a reduction of about 14%. Because the gap enters the conductivity relation exponentially, a narrowing of this size implies a substantial increase in the intrinsic charge-carrier population and hence a strong, easily measurable resistance drop [36]; for comparison, gap changes of only 0.1–0.2% have been judged too small to constitute a useful sensing response in other nanomaterials [36]. The lower band-gap value indicates a less chemically stable and more reactive state, which in organic semiconductors is associated with more facile charge injection and improved device response. This is the quantitative basis for the central prediction of this study: COF_2 adsorption increases the electrical conductivity of thiophene, making the monomer suitable for application in organic cells and organic light-emitting diodes.

CNCl and BF_3: conductivity decrease. CNCl also contributes to the LUMO; its HOMO energy decreases by 0.344 eV (−6.610 → −6.954 eV) and its LUMO by 0.3423 eV (−0.6397 → −0.982 eV), leaving the gap essentially unchanged at 5.972 eV. For BF_3, the fluorine atoms contribute to the LUMO; the HOMO energy increases by 0.222 eV (−6.610 → −6.832 eV) and the LUMO by 0.1924 eV (−0.6397 → −0.8321 eV), widening the gap slightly to 6.00 eV. The widened gap implies reduced conductivity and increased chemical stability, so exposure to these two gases would register as a resistance increase rather than a decrease [37].

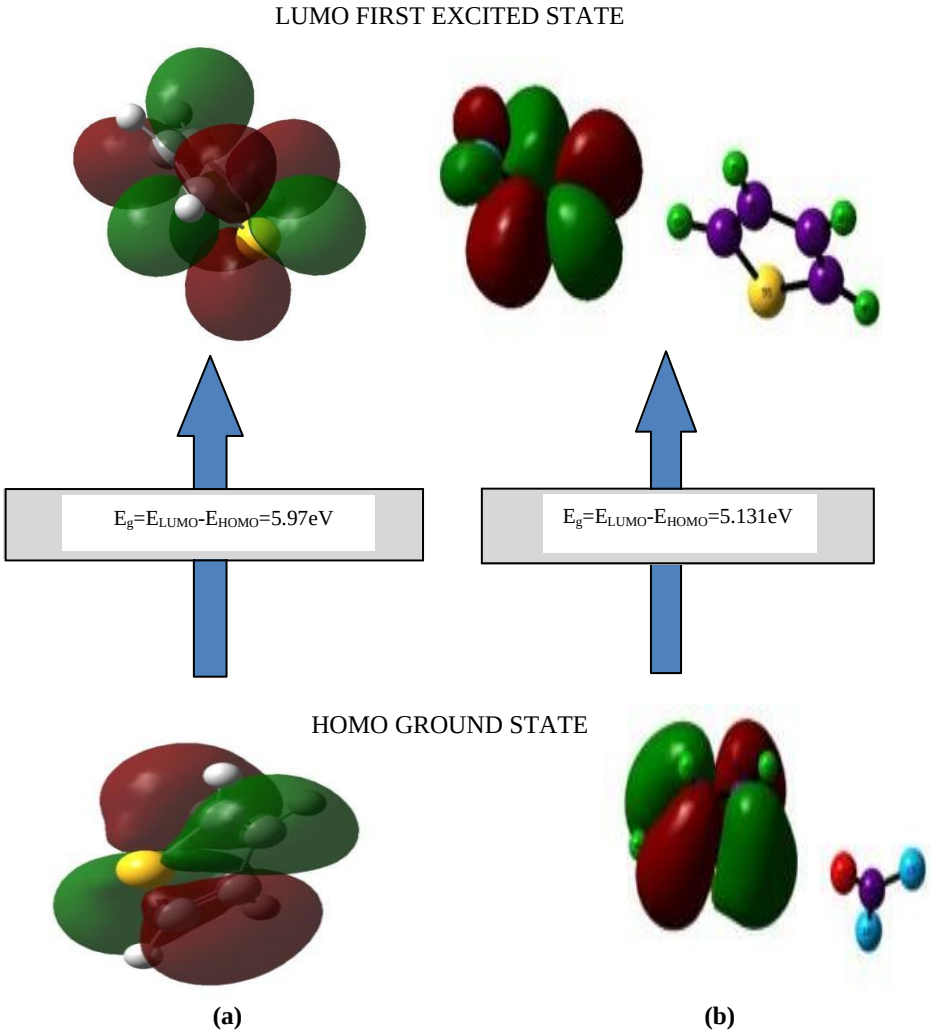


Figure 5. (a). Frontier molecular orbitals for thiophene, and (b) thiophene with COF_2 at the DFT B3LYP/6-31+G (d) level.

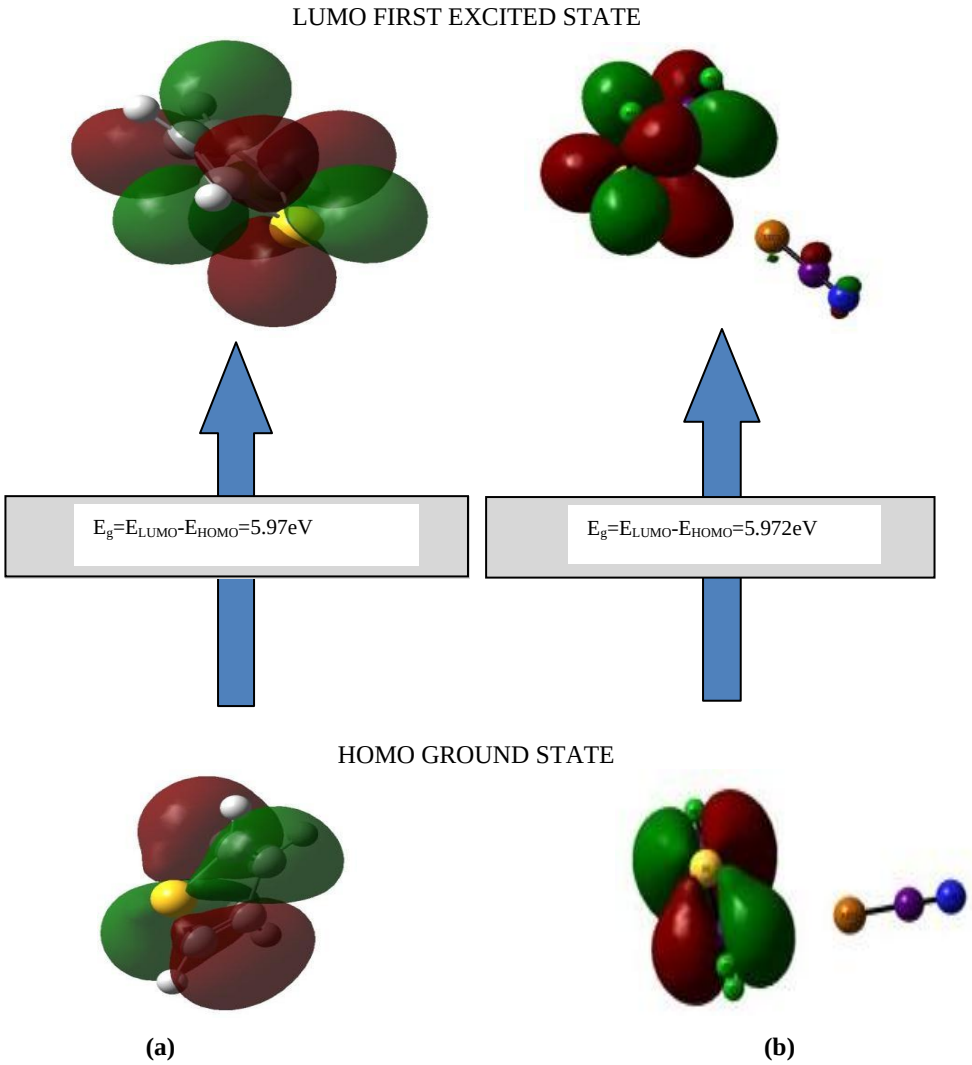


Figure 6. (a). Frontier molecular orbitals for thiophene, and (b) thiophene with CNCl at the DFT B3LYP/6-31+G (d) level.

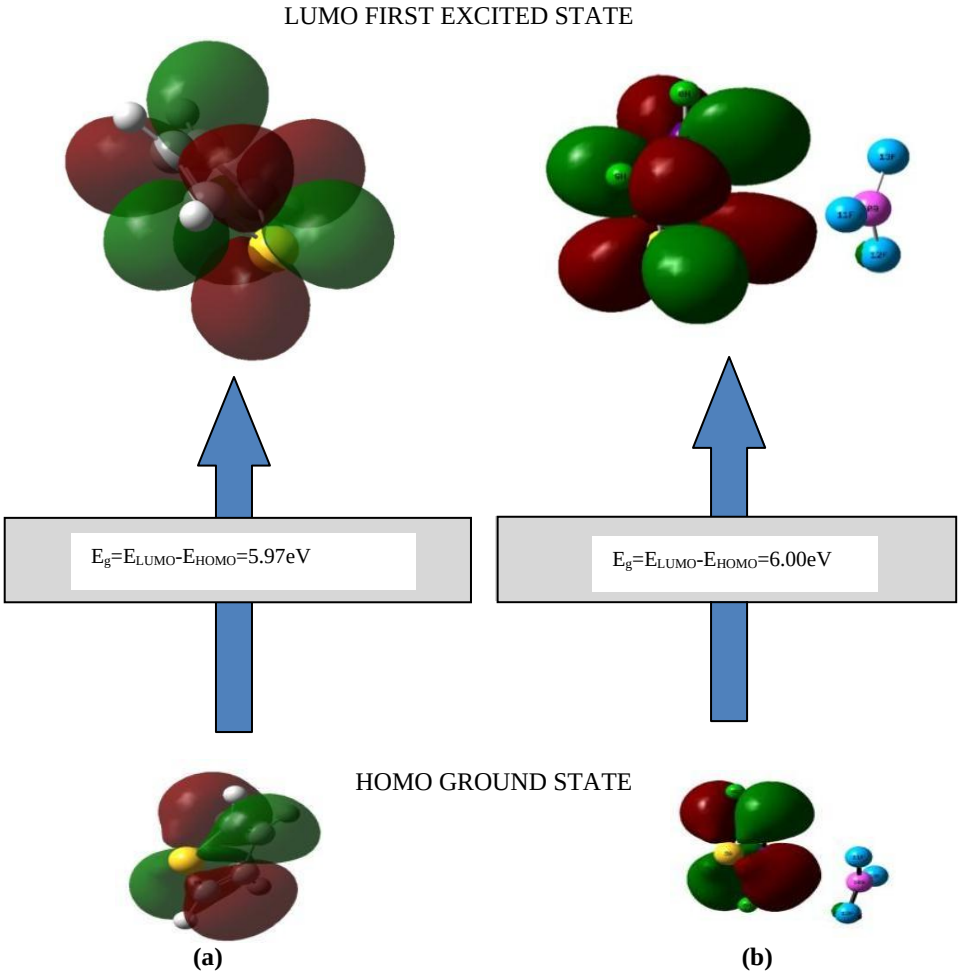
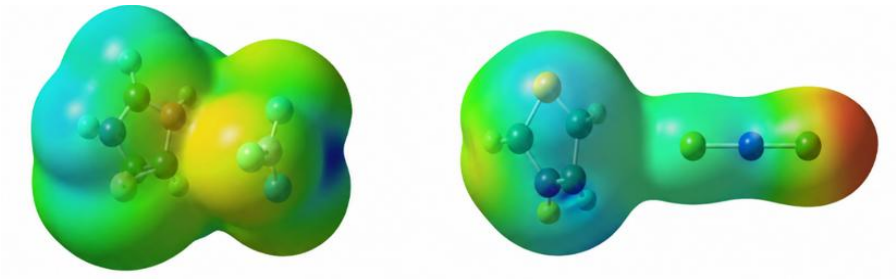


Figure 7. Frontier molecular orbitals for thiophene, and (b) thiophene with BF_3 at the DFT B3LYP/6-31+G(d) level.

Two design insights follow. First, the direction of the resistance change is analyte-selective: COF_2 produces a conductivity increase while CNCl and BF_3 produce a decrease (or near-null change), so a single thiophene element or a small thiophene/polythiophene array can discriminate COF_2 from the other two gases purely from the sign of the response, a form of selectivity without functionalization. Second, the analyte orbital participation determines the transduction channel: in every complex the analyte contributes to the LUMO (the COF_2 and CNCl molecules and the fluorine atoms of BF_3), meaning the lowest unoccupied level of the device acquires adsorbate character upon exposure. Such localization of the LUMO on the adsorbate is recognized in the broader DFT gas-sensing literature as direct evidence of a strong interaction with notable charge transfer, and it provides a low-energy acceptor state that facilitates electron transfer between the film and the analyte [39]. The ordering and directionality of these effects a large, unique gap narrowing for COF_2 and small opposing changes for CNCl/BF_3 constitute the central, practically actionable result of the energy-gap analysis.

Molecular electrostatic potential

The molecular electrostatic potential is an effective tool for predicting sites and reactivities toward both electrophilic and nucleophilic attacks. The adsorption performance of the complexes is evaluated by mapping the total electron density with the MEP of thiophene and the thiophene–analyte complexes, as shown in Figures 8(a), 8(b), 9, and 10. The color-code range is between $-2.311e^{-2}$ (red) and $2.311e^{-2}$ (blue) for thiophene, $-5.546e^{-2}$ and $5.546e^{-2}$ for thiophene–COF_2, $-4.445e^{-2}$ and $4.445e^{-2}$ for thiophene–CNCl, and $-5.615e^{-2}$ and $5.615e^{-2}$ for thiophene–BF_3. In the isolated monomer, the red region over the carbon atoms marks the favorable electrophilic site; after adsorption this is replaced by yellow/green regions of intermediate potential, indicating redistribution of charge between monomer and analyte in every complex. The broadening of the potential ranges shows the strongest electrostatic perturbation for the BF_3 complex — again consistent with its largest interaction energy.



(a) **(b)**

Figure 8. (a). The total electron density isosurface mapped with the molecular electrostatic potential of thiophene, (b) the total electron density isosurface mapped with the molecular electrostatic potential of thiophene with adsorbed COF_2.



Figure 9. The total electron density isosurface mapped with the molecular electrostatic potential of thiophene with adsorbed CNCl.

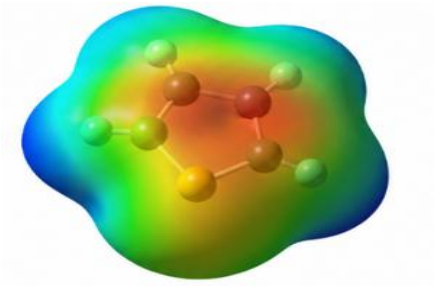


Figure 10. The total electron density isosurface mapped with the molecular electrostatic potential of thiophene with adsorbed BF3 NBO analysis.

Energetic analysis of NBO interactions relies on the use of a one-electron effective energy operator known as the Fock matrix, along with estimates of energetic significance based on second-order perturbation theory calculations. It is widely recognized that certain orbitals act as electron donors while others function as electron acceptors. The findings explore the interaction between occupied donor Lewis-type NBOs and vacant acceptor non-Lewis-type NBOs. These interactions result in a reduction of occupancy from the localized NBOs of the idealized Lewis structure into the vacant non-Lewis orbitals through delocalizations or deviations from the idealized Lewis structure.

In plain terms, NBO analysis recasts the delocalized molecular wave function into localized, chemically intuitive orbitals: Lewis-type orbitals that hold electron pairs (bonds σ/π and lone pairs LP) and vacant non-Lewis orbitals (antibonds σ*/π* and Rydberg orbitals). Second-order perturbation theory then quantifies, through the stabilization energy $E^{(2)}$, how much energy is gained when electron density delocalizes from a filled donor orbital into an empty acceptor orbital. Two regimes are distinguished in all three complexes:

Within thiophene (intramolecular). The dominant delocalizations are the conjugation of the sulfur lone pair into the ring antibonds, LP(S5) → π*(C–C), with $E^{(2)} \approx$ 21-22 kcal/mol, and the π(C–C) → π*(C–C) ring delocalizations at ≈ 15-16 kcal/mol. These large values simply describe the aromatic stabilization of the thiophene ring itself; they are barely perturbed by the presence of the analyte.

Between thiophene and the analyte (intermolecular). The intermolecular $E^{(2)}$ values are two orders of magnitude smaller (0.05-2.13 kcal/mol), confirming that weak, noncovalent interactions stabilize the complexes rather than chemical bonds. Each complex has a characteristic dominant channel. Thiophene–COF_2: the oxygen lone pair of COF_2 donates into the σ*(C1–H6) antibond of thiophene (LP(O11) → σ*(C1–H6), $E^{(2)}$ = 1.20 kcal/mol). This matches the Mulliken/NBO picture in which COF_2 acts as the electron donor. Thiophene–CNCl: the flow is reversed the ring π(C3–C4) bond donates into the σ*(C10–Cl11) antibond of CNCl (0.43 kcal/mol), consistent with thiophene acting as the donor, with a smaller back-donation from the chlorine lone pair LP → π*(C3–C4) (0.12 kcal/mol). Thiophene–BF_3: the π(C1–C2) bond donates into the vacant boron lone-pair orbital LP*(B10) with the largest intermolecular stabilization of the entire study (2.13 kcal/mol), supplemented by weaker π → σ*(B–F) donations (0.06-0.11 kcal/mol) and small reverse fluorine lone-pair donations LP(F) → π*(C1–C2) (0.10-0.12 kcal/mol). The dominance of this channel explains, at the orbital level, why BF_3 binds most strongly and is sensed most readily.

Thiophene with COF_2. Out of all the interacting NBOs, the interaction between the sulfur lone pair and π*(C3–C4) gives the highest stabilization energy of 21.26 kcal/mol. The next strongest stabilization energy of 21.17 kcal/mol is identified for the interaction of the lone pair orbital localized on S5 with π*(C1–C2). Thus, the interaction energy that leads to stabilization arising from the nonbonding interactions enhances the stability of the monomer. The delocalization of electrons from π(C1–C2) to π*(C3–C4) resulted in the next strongest stabilization energy of 15.75 kcal/mol; the delocalization of electrons of π(C3–C4) to π*(C1–C2) gave another strong stabilization energy of 15.28 kcal/mol. Thus, the higher $E^{(2)}$ of thiophene originates from the atomic overlap between LP(S) and π* orbitals and between π and π*, confirming higher intramolecular charge transfer within the monomer.

The NBO analysis of the interaction of thiophene with COF_2 showed three intermolecular interactions (unit-2 to unit-1). The strongest interaction between the lone electron pair of O11 of COF_2 with the antibonding orbital σ*(C1–H6) of thiophene caused a stabilization of 1.20 kcal/mol. Another intermolecular interaction between the π bonding orbital O10–C11 and the Rydberg non-Lewis NBO of H6 caused a stabilization of 0.36 kcal/mol. Another interaction between the lone pair of O11 and the Rydberg non-Lewis NBO of C1 stabilized the complex thiophene–COF_2 by 0.05 kcal/mol. The charge transfer between analyte and monomer is due to the overlapping of the out-of-phase interaction that forms the antibonding σ* type of C1–H6 of

thiophene with the lone electron pair of oxygen of COF_2. No interaction from thiophene to COF_2 exceeded the intermolecular threshold (0.05 kcal/mol), confirming COF_2 as the donor and thiophene as the acceptor, in agreement with the Mulliken and NBO charge transfer results.

Thiophene with CNCl. Out of all the interacting NBOs, the interaction between the sulfur lone pair and π*(C3–C4) gives the greatest stabilization energy of 21.66 kcal/mol. The next strongest stabilization energy of 21.33 kcal/mol is found for the interaction of the lone pair orbital localized on S5 with π*(C1–C2). The delocalization of electrons from π(C1–C2) to π*(C3–C4) leads to a stabilization energy of 15.72 kcal/mol; the delocalization of electrons of π(C3–C4) to π*(C1–C2) gave a stronger stabilization energy of 15.16 kcal/mol. When the stabilization energy is substantial, the interaction between the electron donors and acceptors will be more pronounced, indicating a tendency for the electron donors to donate more electrons to acceptors, which increases the extent of conjugation of the system; this can be identified with increased electron density stabilizing the donor–acceptor interaction.

Regarding thiophene CNCl, the intermolecular hyperconjugative interactions are caused by the orbital overlap between π(C3–C4) of thiophene and σ*(C10–Cl11) of CNCl, giving rise to intermolecular charge transfer leading to stabilization of the system by 0.43 kcal/mol .The prominent charge transfer is noticed from thiophene to CNCl based on Mulliken and NBO charge transfer analysis. However, from the second-order perturbation theory, it is clear that some appreciable amount of electron transfer due to reverse charge transfer occurs between LPCl11 and the antibonding π*(C3–C4), leading to a stabilization of 0.12 kcal/mol

Thiophene with BF_3. Out of all the interacting NBOs, the interaction between the sulfur lone pair and π*(C_3–C_4) gives the strongest stabilization energy of 21.36 kcal/mol. The next strongest stabilization energy of 21.9 kcal/mol is identified for the interaction of the lone pair orbital localized on S5 with π*(C_1–C_2). The delocalization of electrons of π(C_3–C_4) to π*(C_1–C_2) gave a stabilization energy of 15.83 kcal/mol; the delocalization of electrons from π(C_1–C_2) to π*(C_3–C_4) resulted in a stabilization energy of 15.02 kcal/mol.

The second-order perturbation energies corresponding to the hyperconjugative interactions between thiophene and BF_3 showed that there were four intermolecular interactions from thiophene to BF_3, namely π((C_1–C_2) → LP*B10,* π(C_1–C_2) → σ(B_{10}–F_{11}), π(C_1–C_2) → σ*(B_{10}–F_{12}), and π(C_1–C_2) → σ*(B_{10}–F_{13}), leading to stabilization energies of 2.13, 0.06, 0.11, and 0.08 kcal/mol, respectively. In addition, there were two intermolecular interactions where BF_3 acts as a donor NBO and thiophene as an acceptor NBO: the stabilizing energies characterizing LPF12 → π*(C_1–C_2) and LPF13 → π*(C_1–C_2) are 0.1 and 0.12 kcal/mol, respectively. The dominance of the π(C_1–C_2) → LP*(B10) channel — the largest intermolecular stabilization of the entire study (2.13 kcal/mol) — explains, at the orbital level, why BF_3 binds most strongly and is sensed most readily.

Charge transfer: Mulliken and NBO analysis

The charge transfer between thiophene and each analyte quantifies the extent of electron redistribution upon adsorption and corroborates the donor–acceptor directions identified by the NBO second-order analysis above. Basing the interpretation on the charge transfer phenomenon, COF_2 gives −0.0167 e^- to thiophene from Mulliken analysis. The same trend is observed from NBO charge transfer, whereby the analyte gives 0.00218 e^- to the monomer; thus COF_2 acts as the electron donor and transfers charge to thiophene. The low charge values obtained through both Mulliken and NBO analysis are related to a van der Waals kind of interaction, which is in total agreement with the low interaction energy. These charge transfer results agree with the results of the second-order perturbation theory analysis of the Fock matrix of thiophene with COF_2, whereby COF_2 was considered as a donor NBO and thiophene as an acceptor NBO. The charge transfer alters the electronic properties of thiophene and hence proves the sensing capability of the monomer toward the analyte.

The charge transferred between thiophene and CNCl was calculated from the difference between the charge on thiophene after its interaction with CNCl and the charge on the isolated thiophene. Compared with COF_2, a reverse transfer of charge is achieved in the thiophene–CNCl complex: based on Mulliken analysis, thiophene gives 0.0081 e^- to CNCl, and from NBO analysis CNCl accepts 0.00563 e^- from thiophene. These results agree with the second-order perturbation theory analysis of the Fock matrix of thiophene with CNCl, whereby thiophene was considered as a donor NBO and CNCl acts as an acceptor NBO.

For thiophene with BF_3, the interactions are established due to a Mulliken charge transfer of −0.0357 e^- from the analyte to the monomer and, on the other hand, a reverse transfer of charge equal to 0.00912 e^- from monomer to analyte based on NBO analysis. These charge transfer results coincide with the second-order perturbation theory analysis of thiophene with BF_3, whereby BF_3 was considered as a donor NBO and thiophene as an acceptor NBO in agreement with the Mulliken charge transfer; similarly, from the second-order perturbation theory, a reverse transfer of charge takes place, with thiophene acting as a donor NBO and BF_3 as an acceptor NBO, in accordance with the NBO charge transfer.

Limitations

The present calculations refer to an isolated thiophene molecule (the repeating unit of polythiophene) in the gas phase. Effects present in a real sensing film packing of polymer chains, humidity, solvent or substrate polarization, and the oligomeric or periodic electronic structure of polythiophene are therefore not included, and the gas-phase gap of the monomer is expected to differ from that of a thin film. The recovery times assume T = 300 K and an attempt frequency of 1 THz; because $\tau \propto \exp(|E_b|/k_BT)$, operation at other temperatures shifts the desorption times exponentially. Selectivity was assessed only among the three target analytes; competitive co-adsorption of atmospheric constituents (N_2, O_2, CO_2, H_2O) and cross-sensitivity to interfering gases in real sensor environments were not modeled. These aspects define the next stage of this work, which will employ explicit humidity and competitive-adsorption models and oligomeric (and ultimately periodic) polythiophene representations.

CONCLUSION

DFT calculations at the B3LYP/6-31+G(d) and ωB97XD/6-31+G(d) levels of theory for thiophene and its interactions with the analytes (COF_2, CNCl, and BF_3) were performed to explore the potential of thiophene as an effective toxic-gas sensing material. This research indicated that thiophene could act as an efficient gas sensor, potentially replacing traditional solid-state sensors. Both the intermolecular interaction energy and the counterpoise-corrected energies were computed and examined. The intermolecular interaction was identified as a weak van der Waals interaction, and the adsorption energy was within the physisorption range. The recovery-time values suggest the reusable efficiency of the thiophene gas sensor. The Mulliken and NBO calculations quantified the extent of intermolecular charge transfer from monomer to analyte or vice versa, which provides a basis for the sensing capability of thiophene. The conductivity of thiophene increased upon interaction with the analyte COF_2 due to a reduction in the energy-gap value; for the complexation of thiophene CNCl and thiophene–BF_3 interactions, the energy gap of thiophene slightly increases, rendering thiophene more chemically stable and less reactive. The change in conductivity is one of the best indicators to theoretically understand the gas-sensing behavior of thiophene. Frontier molecular orbitals were visualized, providing evidence of atomic-orbital overlap. Molecular electrostatic potential analysis was conducted to understand the electrophilic and nucleophilic attack properties of the complexes. The intramolecular and intermolecular charge transfer occurring between the bonding and antibonding orbitals was determined by second-order perturbation analysis, consistent with the electronic cloud density

results from gas to thiophene or vice versa. All calculations demonstrate the sensing capability of thiophene toward the analytes, with the greatest response toward BF_3 in terms of interaction energy. Thiophene is a promising material that warrants further research to explore its structural and electronic properties for various applications in organic semiconducting devices and as a functional organic material for electronic and optical devices.

ACKNOWLEDGEMENTS

The authors are thankful to KCG College of Technology, Karapakkam, and Madras Christian College, Tambaram, for providing the computational facilities necessary for the pursuit and completion of this work.

REFERENCES

1. Ma, B.; Ren, L.; Liu, G.; Li, J.; Xiao, Y.; Li, D.; Gao, Y.; Kuang, P. A non-dispersive infrared sensor for real-time detection of cyanogen chloride. *S. Afr. J. Chem*. **2022**, 76, 14-19.
2. Munro, N.B.; Talmage, S.S.; Griffin, G.D.; Waters, L.C.; Watson, A.P.; King, J.F.; Hauschild, V. The sources, fate, and toxicity of chemical warfare agent degradation products. *Environ. Health Perspect*. **1999**, 107, 933-974.
3. Nikolić, M.V.; Milovanović, V.; Vasiljević, Z.Ž.; Zoran Stamenkovic. Semiconductor gas sensors: materials, technology, design, and application. Sensors **2020**, 20, 6694-6724.
4. Miasik, J.J.; Hooper, A.J.; Tofield, B.C. Conducting polymer gas sensors. *J. Chem. Soc. Faraday Trans*. 1 1986, 82, 117-1126.
5. Bai, H.; Shi, G. Gas sensors based on conducting polymers. *Sensors* **2007**, 7, 267-307.
6. Cao, Z.; Zhou, G.; Zheng, H.; Liu,Y.;Sun,H.; Zhang,H.; Xu,K. Ultrasensitive chemiresistive sensor for NO_2 based on oxidation of a thiophene polymer bearing oligoethylene glycol side chains. *ACS Appl. Polym. Mater*. **2023**, 5, 9690-9697.
7. Chang, J.B.; Liu, V.; Subramanian, V.; Sivula, K.; Luscombe, C.; Murphy, A.; Liu, J.; Fréchet, J.M.J. Printable polythiophene gas sensor array for low-cost electronic noses. *Appl. Phys. Lett*. **2006**, 88, 014506.
8. Li, B.; Sauvé, G.; Iovu, M.C.; Jeffries-El, M.; Zhang, R.; Cooper, J.; Santhanam, S.; Schultz, L.; Revelli, J.C.; Kusne, A.G.; Kowalewski, T.; Snyder, J.L.; Weiss, L.E.; Fedder, G.K.; McCullough, R.D.; Lambeth, D.N. Volatile organic compound detection using nanostructured copolymers. *Nano Lett*. **2006**, 6, 1598-1602.
9. Bibi, S.; Ullah, H.; Ahmad, S.M.; Shah, A.-u.-H.A.; Bilal, S.; Tahir, A.A.; Ayub, K. Molecular and electronic structure elucidation of polypyrrole gas sensors. *J. Phys. Chem. C* **2015**, 119, 15994-16003.
10. Rad, A.S. Terthiophene as a model sensor for some atmospheric gases: Theoretical study. *Mol. Phys*. **2015**, 114, 584-591.
11. Ullah, H.; Shah, A.-u.-H.A.; Bilal, S.; Ayub, K. DFT study of polyaniline NH_3, CO_2, and CO gas sensors: Comparison with recent experimental data. *J. Phys. Chem. C* **2013**, 117, 23701-23711.
12. Rad, A.S.; Ateni, S.G.; Tayebi, H.-A.; Valipour, P.; Pouralijan Foukolaei, V. First-principles DFT study of SO_2 and SO_3 adsorption on 2PANI: A model for polyaniline response. *J. Sulfur Chem*. **2016**, 37, 622-631.
13. Sajid, H.; Mahmood, T.; Mahmood, M.H.R.; Ayub, K. Comparative investigation of sensor application of polypyrrole for gaseous analytes. *J. Phys. Org. Chem*. **2019**, 32, poc3960.
14. Hossain, M.S.; Saha, J.K. Adsorption of hazardous gases on poly(3,4-ethylenedioxythiophene): Density functional theory study. *Int. J. Chem. Kinet.* **2021**, 53, 121-129.

15. Krishna, P.U.N.; Krishnan, G.S.G.; Muraleedharan, K. Enhanced sensing of SO_3, SO_2, HCN, and CO_2 gases with [2,2′:5′,2″-terthiophene]-3′,4′-diamine: A theoretical study. *Hybrid Adv*. **2024**, 5, 100171.
16. Franco, F.C. Interaction of several toxic heterocarbonyl gases with polypyrrole as a potential gas sensor. *Chemosensors* **2020**, 8, 84-101.
17. Kumaravel, A.; Muthu kumar, K. Risk assessment for chemical in various activities. *Zenodo* **2020**, 3693638.
18. Dorgelo, F.O.; Maclaine Pont, M.A. Health-based recommended occupational exposure limits for carbonylfluoride and PTFE Pyrolysis Products; [Dutch Expert Committee on Occupational Safety (DECOS) / Health Council of the Netherlands]; **1988**.
19. Kumar, V.; Kim, H.; Pandey, B.; James, T.D.; Yoon, J.; Anslyn, E.V. Recent advances in fluorescent and colorimetric chemosensors for the detection of chemical warfare agents: A legacy of the 21st century. *Chem. Soc. Rev*. **2023**, 52, 663-704.
20. Panigrahi, P.; Pal, Y.; Kaewmaraya, T.; Molybdenum carbide mxenes as efficient nanosensors toward selected chemical warfare agents. *ACS Appl. Nano Mater*. **2023**, 6, 8404-8415.
21. Panigrahi, P.; Pal, Y.; Kaewmaraya, T.; Bae, H.; Nasiri, N.; Hussain, T. Molybdenum carbide MXenes as efficient nanosensors toward selected chemical warfare agents. *ACS Appl. Nano Mater*. **2023**, 6, 665-670.
22. Mawwa, J.; Shamim, S.U.D.; Khanom, S.; Hossain, M.K.; Ahmed, F. In-plane graphene/boron nitride heterostructures and their potential application as toxic gas sensors. *RSC Adv.* **2021,** 11, 32810-32823.
23. Becke, A.D. *Density-functional thermochemistry. III. The Role of Exact Exchange. J. Chem. Phys*. **1993**, 98, 5648-5652.
24. Valadi, F.M.; Pasandideh-Nadamani, M.; Rezaee, M.; Torrik, A.; Mirzaie, M.; Torkian, A. Competitive adsorption of CO_2, N_2, and CH_4 in coal-derived asphaltenes, a computational study. *Sci. Rep*. **2024**, 14, 7664.
25. Grimme, S. Density functional theory with london dispersion corrections. *Wires Comput. Mol. Sci*. **2011**, 1, 211-228.
26. Rayón, V.M.; Cabria, I. Assessment of density functional approximations for N_2 And Co_2 physisorption on benzene and graphene. *J. Comput. Chem*. **2022**, 43, jcc.26945.
27. Lazar, P.; Karlický, F.; Jurečka, P.; Kocman, M.; Otyepková, E.; Šafářová, K.; Otyepka, M. Adsorption of small organic molecules on graphene. *J. Am. Chem. Soc*. **2013**, 135, 6372-6377.
28. Henley, A.; Lennox, M.J.; Easun, T.L.; Moreau, F.; Schröder, M.; Besley, E. Computational evaluation of the impact of incorporated nitrogen and oxygen heteroatoms on the affinity of polyaromatic ligands for carbon dioxide and methane in metal–organic frameworks. *J. Phys. Chem. C* **2016**, 120, 27342-27348.
29. Civalleri, B.; Maschio, L.; Ugliengo, P.; Zicovich-Wilson, C.M. Role of dispersive interactions in the CO adsorption on MgO(001): Periodic B3LYP calculations augmented with an empirical dispersion term. *Phys. Chem. Chem. Phys*. **2010**, 12, 6382-6386.
30. Ramzan, M.S.; Kuc, A.B.; Kim, H.S. Electronic fingerprint mechanism of NO_x sensor based on single-material SnP_3 logical junction. *npj Comput. Mater*. **2022**, 8,220.
31. Shahriar, R.; Hassan, O.; Alam, M.K. Adsorption of gas molecules on buckled gaas monolayer: A first-principles study. *RSC Adv*. **2022**, 12,16372-16744.
32. Agrawal, A.V.; Kumar, N.; Kumar, M. Strategy and future prospects to develop room-temperature-recoverable NO_2 gas sensor based on two-dimensional molybdenum disulfide. *Nano-Micro Lett*. **2021**, 13, 38.
33. Kalwar, B.A.; Wang, F.; Soomro, A.M.; Naich, M.R.; Saeed, M.H.; Ahmed, I. Highly sensitive work function type room temperature gas sensor based on Ti doped hBN monolayer for sensing CO_2, CO, H_2S, HF and NO. A DFT study. *RSC Adv*. **2022**, 12, 34185-34199.
34. Yong, Y.; Cui, H.-L.; Zhou, Q.; Su, X.; Kuang, Y.; Li, X. Adsorption of gas molecules on a graphitic gan sheet and its implications for molecule sensors. *RSC Adv*. **2017**, 7, 51027-51035.

35. Aetizaz, M.; Ullah, F.; Sarfaraz, S.; Mahmood, T.; Ayub, K. Robust and facile detection of formaldehyde through transition metals doped olympicene sensors: A step forward DFT investigation. *RSC Adv*. **2023**, 13, 29231-29241.
36. Xu, Z. Adsorption and sensing mechanisms of Ni-Doped $Ptte_2$ monolayer upon NO_2 and O_3 in air-insulated switchgears. *RSC Adv*. **2023**, 13, 18129-18137.
37. Chai, J.-D.; Head-Gordon, M. Long-range corrected hybrid density functionals with damped atom–atom dispersion corrections. *Phys. Chem. Chem. Phys*. **2008**, 10, 6615-6633.